Deep seismic structure of the Tonga subduction zone: Implications for mantle hydration, tectonic erosion, and arc magmatism

Eduardo Contreras-Reyes,[1] Ingo Grevemeyer,[2] Anthony B. Watts,[3] Ernst R. Flueh,[2] Christine Peirce,[4] Stefan Moeller,[2] and Cord Papenberg[2]

Received 8 April 2011; revised 9 July 2011; accepted 15 July 2011; published 13 October 2011.

[1] We present the first detailed 2D seismic tomographic image of the trench-outer rise, fore- and back-arc of the Tonga subduction zone. The study area is located approximately 100 km north of the collision between the Louisville hot spot track and the overriding Indo-Australian plate where ~80 Ma old oceanic Pacific plate subducts at the Tonga Trench. In the outer rise region, the upper oceanic plate is pervasively fractured and most likely hydrated as demonstrated by extensional bending-related faults, anomalously large horst and graben structures, and a reduction of both crustal and mantle velocities. The 2D velocity model presented shows uppermost mantle velocities of ~7.3 km/s, ~10% lower than typical for mantle peridotite (~30% mantle serpentinization). In the model, Tonga arc crust ranges between 7 and 20 km in thickness, and velocities are typical of arc-type igneous basement with uppermost and lowermost crustal velocities of ~3.5 and ~7.1 km/s, respectively. Beneath the inner trench slope, however, the presence of a low velocity zone (4.0–5.5 km/s) suggests that the outer fore-arc is probably fluid-saturated, metamorphosed and disaggregated by fracturing as a consequence of frontal and basal erosion. Tectonic erosion has, most likely, been accelerated by the subduction of the Louisville Ridge, causing crustal thinning and subsidence of the outer fore-arc. Extension in the outer fore-arc is evidenced by (1) trenchward-dipping normal faults and (2) the presence of a giant scarp (~2 km offset and several hundred kilometers long) indicating gravitational collapse of the outermost fore-arc block. In addition, the contact between the subducting slab and the overriding arc crust is only 20 km wide, and the mantle wedge is characterized by low velocities of ~7.5 km/s, suggesting upper mantle serpentinization or the presence of melts frozen in the mantle.

Citation: Contreras-Reyes, E., I. Grevemeyer, A. B. Watts, E. R. Flueh, C. Peirce, S. Moeller, and C. Papenberg (2011), Deep seismic structure of the Tonga subduction zone: Implications for mantle hydration, tectonic erosion, and arc magmatism, *J. Geophys. Res.*, *116*, B10103, doi:10.1029/2011JB008434.

1. Introduction

[2] The amount of volatiles stored within the subducting oceanic lithosphere play a crucial role in arc volcanism and metamorphism of the overlying mantle wedge. At depths between ~60–80 km, dewatering of subducting oceanic crust largely occurs by metamorphism of the oceanic crust to amphibolite and eclogite facies, which leads to hydration of the mantle wedge [*ANCORP Working Group*, 1999; *Ruepke et al.*, 2004; *Hacker et al.*, 2003]. At depths of 100–120 km, eclogitization is complete [*Hacker et al.*, 2003]. The subducting lithospheric mantle dehydrates at a elevated temperature which results in partial melting of the overriding mantle, and which generates magmas that buoyantly rise to form the associated island arc [*Ulmer and Trommsdorff*, 1995; *Ruepke et al.*, 2004]. Thus, the amount of water subducted dictates the generation of arc magmas, the rheology of the mantle wedge, and the global circulation of water [e.g., *Hacker*, 2008].

[3] The amount of fluids stored within the incoming/subducting plate is linked to hydration and alteration of oceanic lithosphere prior to subduction. The process commences at the mid-ocean ridge where, at slow spreading centers, oceanic lithosphere is characterized by a crust and uppermost mantle that are pervasively fractured and hydrated [e.g., *Carbotte and Scheirer*, 2004]. In contrast, oceanic lithosphere created at moderate to fast spreading mid-ocean ridges, such as most of the oceanic plate consumed at Circum-Pacific subduction zones, is characterized by pervasive fracturing and hydrothermal activity largely confined to upper crustal levels [*Carbotte and Scheirer*, 2004]. Lower crust and mantle rocks are, therefore, relatively dry and

[1]Departamento de Geofísica, Facultad de Ciencias Físicas y Matemáticas, Universidad de Chile, Santiago, Chile.
[2]IFM-GEOMAR, Leibniz-Institut für Meereswissenchaften an der Universität Kiel, Kiel, Germany.
[3]Department of Earth Sciences, University of Oxford, Oxford, UK.
[4]Department of Earth Sciences, Durham University, Durham, UK.

0148-0227/11/2011JB008434

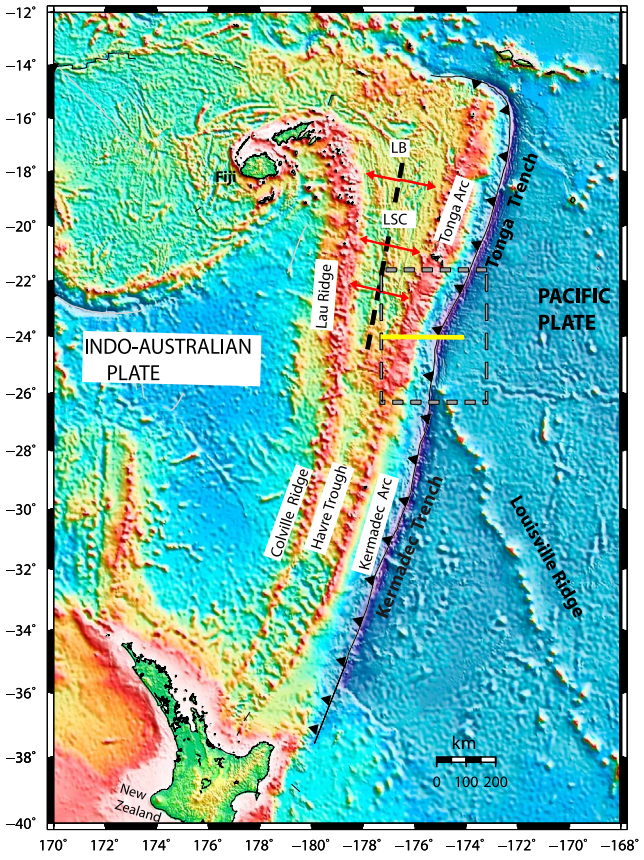

Figure 1. Bathymetric map of the Tonga-Kermadec subduction zone [*Sandwell and Smith*, 1997]. The Pacific plate approaches the Tonga-Kermadec Trench at a fast convergence rate of ~200 mm/a [*Bevis et al.*, 1995], while the spreading rate at the Lau spreading center (LSC) is about 240 mm/a. Dotted square and yellow line denotes the study area and seismic line, respectively (Figure 2). The gentle trench slope south of the modern collision zone between the Louisville Ridge and Tonga-Kermadec Trench (~26°S), is much broader than the steep narrow fore-arc north of the collision. North of the collision zone the trench axis is extremely deep, reaching 10850 m in the Horizon Deep, adjacent to which the trench slope has a very high gradient (>10° below 6000 m; Lonsdale, 1986). In contrast, south of the collision zone, where the trench shallows to 6000 m, the fore-arc is broader, has a more gentle slope (1°–2°), and descends to only 8000 m [*Lonsdale*, 1986]. The geometry suggests that passage of the Louisville Ridge caused a significant amount of erosion to the outer edge of the fore-arc, compared to the normal steady state subduction environment [*Ballance et al.*, 1989].

undeformed [*Carlson*, 2003]. However, a number of observations suggest that this characteristic of a relatively "dry" and "undeformed" oceanic lithosphere, is dramatically perturbed at the outer rise, seaward of the trench [*Grevemeyer et al.*, 2007; *Contreras-Reyes et al.*, 2008; *Ivandic et al.*, 2008]. These authors have suggested that much of the hydration will occur in the trench-outer rise area, when reactivated shallow and new fault grow to penetrate through the crust and into the upper mantle.

[4] The degree of serpentinization of the oceanic mantle has been inferred from seismic wide-angle data for relative young oceanic lithosphere such as in off Middle America (<30 Ma) [*Grevemeyer et al.*, 2007; *Ivandic et al.*, 2008], off south-central Chile (10–30 Ma) [*Contreras-Reyes et al.*, 2008; *Contreras-Reyes and Osses*, 2010], and for relative old plates such as Nazca off north Chile (45–50 Ma) [*Sallares and Ranero*, 2005]. Furthermore, deep mantle refracted seismic waves were used to study the maximum depth of mantle serpentinization off south-central Chile [*Contreras-Reyes et al.*, 2008]. These results show that low mantle velocities associated with mantle serpentinization occur down to a maximum depth of 6–8 km into the upper mantle. At these depths, mantle temperatures are estimated to be ~430°C according to the cooling plate model of *Parsons and Sclater* [1977] or 300–350°C according to the most recent model of *McKenzie et al.* [2005]. The corresponding depths to these isotherms coincide with the neutral surface, or lower limit of the extensional upper region of the oceanic lithosphere, according to focal mechanisms studied in various outer rise settings [e.g., *Seno and Yamanaka*, 1996]. Since water infiltration is confined to the upper extensional part and not to the lower compressional part of the oceanic lithosphere, the neutral surface is consistently the deepest limit of mantle serpentinization.

[5] The Tonga-Kermadec island arc-trench system in the southwest Pacific Ocean (Figure 1) is characterized by: (1) subduction of old oceanic lithosphere (≥80 Ma), (2) a sediment-starved deep-sea trench, (3) highly active arc magmatism and (4) the presence of well-developed extensional faults in the seaward wall of the trench [*Lonsdale*, 1986; *Ballance et al.*, 1989; *Collot and Davy*, 1998]. Such a setting offers the opportunity to study hydration and dehydration processes of the oceanic lithosphere at the outer rise and beneath the magmatic arc, respectively.

[6] A fundamental change in the depth and curvature of the Tonga-Kermadec Trench occurs near the subducting Louisville hot spot track [*Lonsdale*, 1986; *Ballance et al.*, 1989]. The collision zone between the Louisville Ridge and the Tonga-Kermadec Trench is migrating rapidly southward (>220 km/m.y.) due to the oblique and fast convergence rate of the subducting Pacific plate beneath the Indo-Australian plate (~200 km/m.y.) [*Bevis et al.*, 1995]. On the other hand, the overriding outer Indo-Australian fore-arc shows the typical features of a margin affected by tectonic erosion: (1) a sedimented starved trench, (2) the absence of a sedimentary wedge, (3) unfilled horst and graben structures on the incoming oceanic plate and (4) a steep and highly fractured inner trench slope [*Ballance et al.*, 1989]. *Clift and MacLeod* [1999] have shown that the trench slope has subsided to great depths since 32–34 Ma, due to tectonic erosion processes. Moreover, trench-slope subsidence in the post-collision zone was most likely accelerated by the subduction of the Louisville Ridge [*Ballance et al.*, 1989]. As a consequence, intense subsidence of the outermost fore-arc has lead to the formation of the second deepest trench on earth (~10850 m depth).

[7] In addition, the velocity structure of the Tonga arc crust contains important information on how island arcs form. Island arcs have been proposed as a principal site of continental crust genesis [*McLennan and Taylor*, 1982] and, since the bulk composition of continental crust is andesitic,

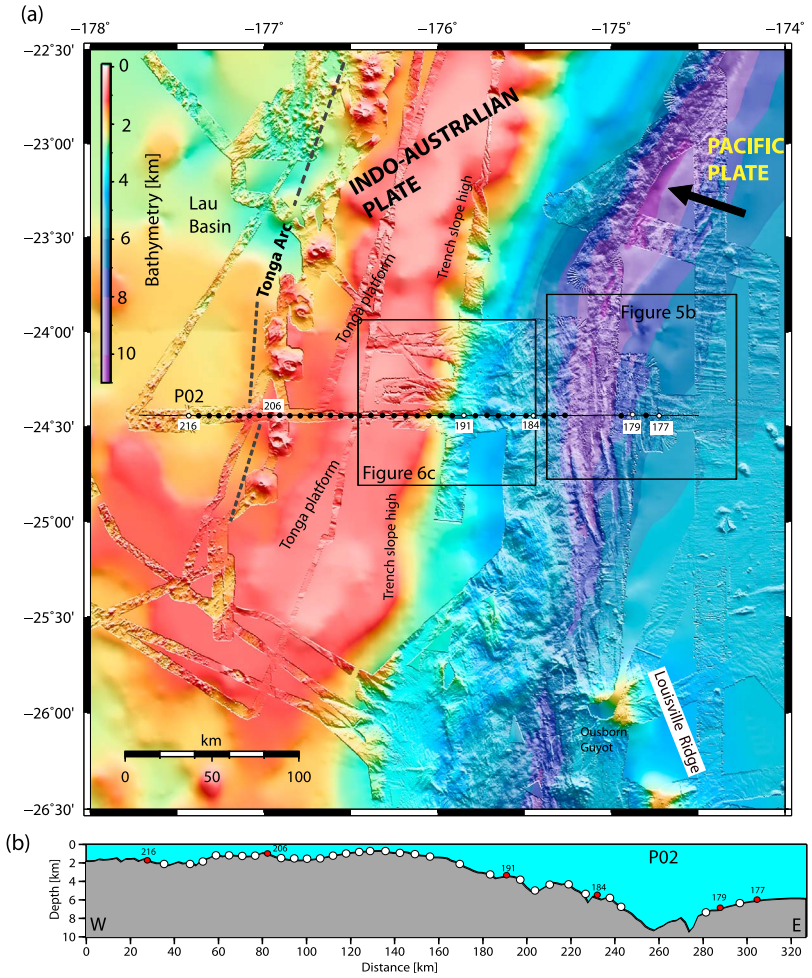

Figure 2. Swath bathymetry data (A.A.P. Koppers, personal communication, 2009) of the Pacific plate and easternmost portion of the Tonga arc. The location of the wide-angle seismic profile is shown. White dots indicate the six OBS stations (216, 206, 191, 184, 179 and 177) of which data examples are shown in Figure 3. The active Tonga arc is parallel and located at roughly 180 km from the trench axis, whereas the Tonga platform forms the widest part of the fore-arc (60–80 km wide) and is composed of a series of volcaniclastic sediments, pelagic chalk and carbonate debris, and overlies an Eocene volcanic basement [*Clift et al.*, 1998]. The trench slope high is the shallowest part of the fore-arc.

the andesite model has been suggested to explain the initial composition of oceanic arc crust [*McLennan and Taylor*, 1982]. Growing geophysical evidence, however, suggests that their seismic structure is closer to basaltic rather than andesitic, which is the average composition of continental crust (e.g., the Aleutian [*Holbrook et al.*, 1999] and Mariana [*Calvert et al.*, 2008] arcs). Intracrustal melting and pervasive deformation have been proposed as a possible solution to this paradox [e.g., *Holbrook et al.*, 1999].

[8] In order to determine the deep lithospheric structure of the Tonga subduction zone, we carried out a wide-angle seismic refraction experiment between January and February 2008 during cruise SO195 of the German R/V *SONNE* (Figure 2). A single seismic profile traversed the entire subduction zone system, including the incoming plate, trench axis, fore-arc and magmatic arc. The profile is ~330 km long and 40 ocean-bottom seismograph (OBS) stations were deployed in water depths up to 8000 m. The profile is located ~100 km north of the collision zone between the Louisville Ridge and the Tonga Trench and therefore, sampled, an island arc affected by the subduction of the Louisville Ridge during the last few million years. The results of this seismic study may offer insights into deep lithospheric hydration, arc magmatism, arc crust formation and tectonic evolution and erosion of the overriding plate.

2. Tectonic Setting

[9] The Tonga-Kermadec system represents a classic example of a non-accretionary convergent margin in an intraoceanic setting. Here, subduction is believed to date from the middle Eocene on the basis of the oldest volcanoclastic strata that have been found in the fore-arc region [*Clift et al.*, 1998, and references therein]. This region comprises zones of island arc magmatism, back-arc rifting, and seafloor spreading (Figure 1). The Pacific plate subducts beneath the Indo-Australian plate at the Tonga-Kermadec Trench at a fast convergence rate of 200–250 mm/a which

Table 1. Summary of Travel Time Picks and Details of the Average Final Velocity Depth Model Shown in Figure 4c[a]

Phase	Average Travel Time Uncertainty (ms)	Average Final Model T_{RMS} (ms)	Average Final Model χ^2
$P_{g1} + P_{m1}P$	55	55.58	1.06
P_{n1}	60	56.27	0.93
$P_{tsc}P$	80	76.44	0.94
$P_{g2} + P_{m2}P$	55	57.59	1.11
P_{n2}	60	53.32	0.89

[a]P_{g1}, arc crustal refraction; $P_{m1}P$, reflections from the upper plate Moho, P_{n1} forearc mantle refractions, $P_{tsc}P$ reflection from the top of the oceanic crust; P_{g2}, refraction from the lower plate crust; $P_{m2}P$, reflections from the lower plate Moho; P_{n2}, lower plate mantle refractions; T_{RMS}, root-mean square travel time misfit; and χ^2, chi-square parameter.

increases northward [*Bevis et al.*, 1995], and partial melting generates magmas that migrate upward to form the Tonga and Kermadec volcanic arcs.

[10] The Miocene-Recent Lau-Havre back-arc basin between the active Tonga-Kermadec arc and the remnant Lau-Colville Ridge is the central rift of a ~700 km long mid-ocean ridge system (Figure 1) [*Karig*, 1970]. ODP drill sites indicate that back-arc rifting began at 7 Ma, pre-dating seafloor spreading [*Shipboard Scientific Party*, 1992]. Current back-arc opening rates decrease from 159 mm/yr in the northern Lau Basin to 15 mm/yr in the southern Havre Trough [*Bevis et al.*, 1995]. The V-shaped Lau Basin currently opens at two overlapping, southward propagating spreading centers. The Havre Trough has low seismicity and volcanic basement ridges trending 25–45° oblique to the basin axis, consistent with low levels of extensional tectonism and volcanism [*Ruellan et al.*, 2003].

[11] The Tonga-Kermadec arc contains an active and a remnant volcanic chain (Figure 1). The eastern, remnant chain includes the coral islands of the Tonga group and consists of uplifted carbonates and gravity flow sediment deposits over middle Eocene to late Miocene volcanic and plutonic rocks [*Karig*, 1970]. The western, active Tofua chain formed 0–3 Myr ago [*Karig*, 1970] and is made up of basaltic seamounts, shoals and rocky islands. On the fore-arc to the east, Miocene sediments are down-faulted against flows and tuff breccias which are believed to have been part of a prior island arc system [*Hawkins*, 1995].

[12] The Tonga-Kermadec island arc-trench system is marked by widespread tectonic erosion of the overriding plate by the subducting oceanic Pacific lithosphere. At the trench, there is no accretionary wedge, and the trench contains less than 0.2 km of sediments [*Ballance et al.*, 1989]. The seaward wall of the trench is steep and highly fractured [*Lonsdale*, 1986; *Ballance et al.*, 1989; *MacLeod*, 1994]. At ~26°S, the Louisville Ridge intersects the trench thereby separating the Tonga Trench in the north from the Kermadec Trench in the south (Figure 1). The Louisville Ridge is a ~4000 km long chain of seamounts which is believed to have formed while the Pacific plate moved over a hot spot, which is presently located near the intersection of the Eltanin Fracture Zone and the SW Pacific-Antarctica Ridge [*Lonsdale*, 1986; *Watts et al.*, 1988]. Near its intersection with the Tonga-Kermadec Trench, the incoming Louisville seamounts rise some 4–5 km above the surrounding seafloor causing a local shallowing in the depth of the trench (5–6 km depth). The Osbourn seamount, which has a once flat surface that has been tilted down toward the trench, is apparently the next volcanic edifice to intersect the trench (Figure 2). The point of intersection is moving rapidly southward at rates faster than 200 km/Ma. Tectonic erosion has accelerated in the wake of Louisville Ridge subduction, which causes frontal and basal erosion processes and regional subsidence of the easternmost part of the overriding plate [*Ballance et al.*, 1989; *Clift et al.*, 1998].

3. Wide-Angle Seismic Data

[13] Seismic refraction data were acquired during R/V *SONNE* cruise 195. Profile P02 is 327 km long and 40 OBS were deployed along it at approximately 8 km spacing (Figure 2). Four of the 40 stations failed to record data. The seismic source was an airgun array comprising 6 G-gun clusters with a total volume of 81 liters, fired at 210 bar pressure every 60 s at a surveying speed of 5 kn, yielding a shot spacing of ~150 m. For all record sections, a time and offset-variable Butterworth filter, in which the passband moves toward lower frequencies as record time and offset increase, was applied to account for frequency changes caused by signal attenuation.

[14] In the overriding plate, we recorded intracrustal refractions (P_{g1}), Moho reflections ($P_{m1}P$), and upper-mantle refractions (P_{n1}). $P_{m1}P$ and P_{n1} phases were observed on eight instruments, at offsets up to 120 km. On the incoming oceanic plate, crustal (P_{g2}) and mantle refractions (P_{n2}), and some reflections from the top ($P_{tsc}P$) and bottom ($P_{m2}P$) of the subducting Pacific crust were identified (see Table 1 for details of the travel time arrivals and picking errors). Additionally, deep-seated reflections (DSR) within the upper mantle were observed at some stations. Six example record sections are shown in Figure 3, with their identified seismic phases annotated.

4. Seismic Tomography

[15] The 2D velocity structure along seismic profile P02 was determined using a joint refraction and reflection travel-time inversion technique [*Korenaga et al.*, 2000]. This method allows joint inversion of seismic refraction and reflection travel-time data for a 2-D velocity field. Travel times and raypaths are calculated using a hybrid ray-tracing scheme based on the graph method and the local ray-bending refinement [*Van Avendonk et al.*, 1998]. Smoothing constraints, using pre-defined correlation lengths and optimized damping constraints for the model parameters, are employed to regularize an iterative linearized inversion [*Korenaga et al.*, 2000].

[16] The velocity model consists of the following layers: (1) water, (2) sediments on the overriding plate, (3) arc crust, (4) uppermost fore-arc mantle, and (5) subducting oceanic crust and mantle. To derive the velocity-depth model the water depth, taken from the swath bathymetry center beam, was used to construct the seabed-water column interface, and this remained fixed during the inversion. In order to obtain the sedimentary and crustal velocities, and Moho depths of the overriding plate, we jointly inverted

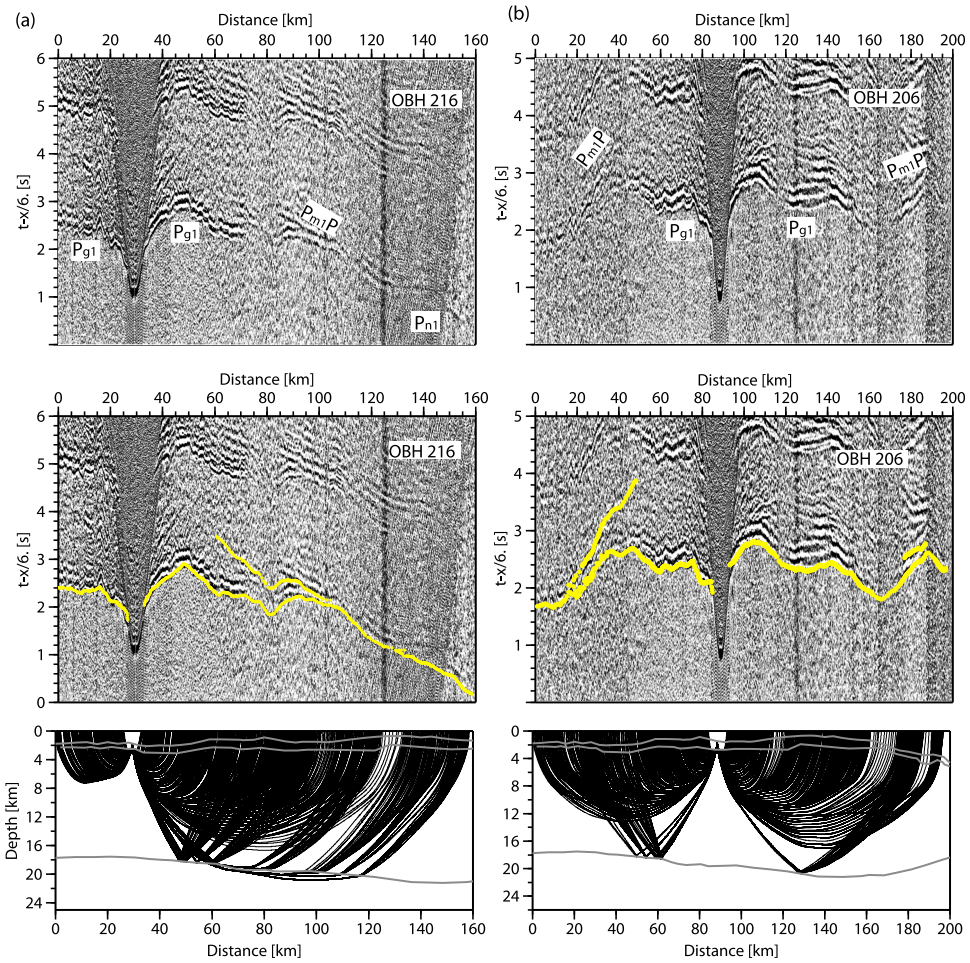

Figure 3. Examples of wide-angle seismic data with predicted travel times (yellow curves), which are computed based on the velocity model presented in Figure 4c. (a) OBH 216, (b) OBH 206, (c) OBH 191, (d) OBS 184, (e) OBS 179, and (f) OBS 177. Orange dotes in Figures 3c–3f correspond to travel times predicted by the final velocity model shown in Figure 4c that were not included in the tomographic inversion.

refraction (P_{g1}) and reflection ($P_{m1}P$) phases. The arc crust velocities and Moho depths derived from the tomographic inversion were then held fixed in the following iterative inversions. Mantle wedge velocities were inverted using P_{n1} phases, while the top of the subducting oceanic crust was constrained using $P_{tsc}P$ arrivals. Similarly, mantle wedge velocities and the interplate boundary depth remained fixed for the next step of the inversion, where crustal velocities and Moho depths of the subducting Pacific crust were derived using oceanic P_{g2} and $P_{m2}P$ phases, respectively. Finally, the uppermost mantle velocities of the incoming Pacific plate were inverted using P_{n2} phases. It is worth noting that this layer-stripping approach [*Zelt*, 1999] uses both first and second arrivals to constrain the velocity model, without the need to disregard for example, secondary arrivals such as lower crustal phases which become secondary arrivals at offsets where mantle arrivals become the first arriving phase.

4.1. Reference Model and Inversion Parameters

[17] In order to start the iterative process of linearized inversion, a good reference model is needed to ensure stable inversion of the parameters. The reference 2D velocity model is 327 km long and 36 km deep. We used three floating reflectors to model (1) the Moho of the overriding arc crust, (2) the top of the subducting Pacific crust and (3) the Moho of the Pacific oceanic crust. Initial crustal and mantle velocities of the Indo-Australian plate were obtained by forward modeling the $P_{g1}P$ and P_{n1} refraction phases, respectively. The initial geometry of the Moho of the overriding arc crust and interplate boundary reflector were obtained by forward modeling the $P_{m1}P$ and $P_{tsc}P$ reflections, respectively. Similarly, the initial crustal and mantle velocities of the oceanic Pacific plate were obtained by forward modeling the $P_{g2}P$ and P_{n2} refracted phases. The initial Pacific crustal thickness was obtained by forward modeling the $P_{m2}P$ reflections. We prepared the reference model for the tomographic inversion by first 1-D modeling three OBS stations, which we consider key to defining the general velocity-depth structure. Figure 4a shows the 1-D models of the three selected stations. The 2-D seismic velocities of the reference model are calculated by linearly interpolating the velocities of these 1-D velocity models to form the starting model.

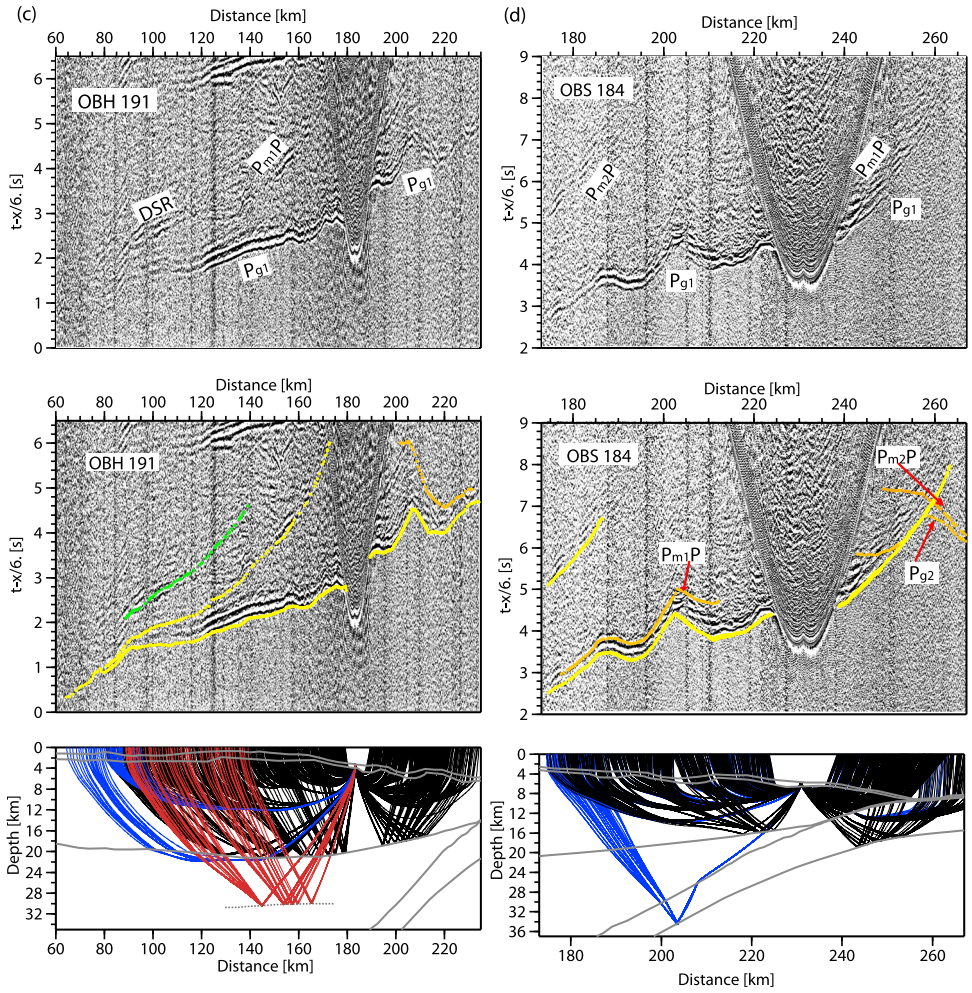

Figure 3. (continued)

[18] Unfortunately, reflections from the top of the subducted oceanic crust were clearly observed in only four stations making modeling difficult. However, we forward modeled $P_{m2}P$ phases that were identified in a larger number of stations in order to derive the bottom of the subducted crust first. Thus, we infer the geometry of the top of the subducted crust by just subtracting a constant thickness of ~6.0 km to the derived Moho of the subducting crust. The constant thickness of 6.0 km is the average crustal thickness of the Pacific crust derived east of the trench by modeling $P_{m2}P$ reflections (see for instance Figure 3f).

[19] The horizontal grid spacing of the model used for the velocity inversion is 0.5 km, whereas the vertical grid spacing is varied from 0.1 km at the top of the model to 1 km at the bottom. Depth nodes defining the plate boundary and Moho reflectors are spaced at 1 and 2 km, respectively. We used horizontal correlation lengths (input parameters for the regularization of the inversion) ranging from 2 km at the top to 10 km at the bottom of the model, and vertical correlation lengths varying from 0.1 km at the top, to 2.5 km at the bottom. Different tests showed that varying the values of correlation lengths by 50% does not significantly affect the solution. Due to the trade-off between correlation lengths and smoothing weights, we tried to use shorter correlation length and larger smoothing weight in order to reduce memory requirements [*Korenaga et al.*, 2000]. Depth and velocity nodes are equally weighted in the refraction and reflection travel time inversions.

4.2. Velocity Model Uncertainties

[20] Interpretation of the best-fit velocity model requires knowledge of model uncertainties. To determine the accuracy of the final model, we employed the Monte Carlo method [*Korenaga et al.*, 2000]. To estimate velocity-depth uncertainties, we randomly perturbated the velocities and reflector-depths of our reference model (Figure 4a). We generated 10 random initial velocity models by adding randomly distributed smooth perturbations (maximum velocities perturbations of ±0.5 km/s at the top and ±0.2 km/s at the bottom of the overriding and Pacific crusts, with wavelength perturbations of 10 km horizontally and 0.5 km vertically). For both plates, mantle perturbation was ±0.2 km/s, with wavelength perturbations of 20 km horizontally and 1 km vertically. The initial geometries of the interplate and Moho reflectors were randomly varied within a range of ±1.5 km. In addition to the perturbed reference models, we produced

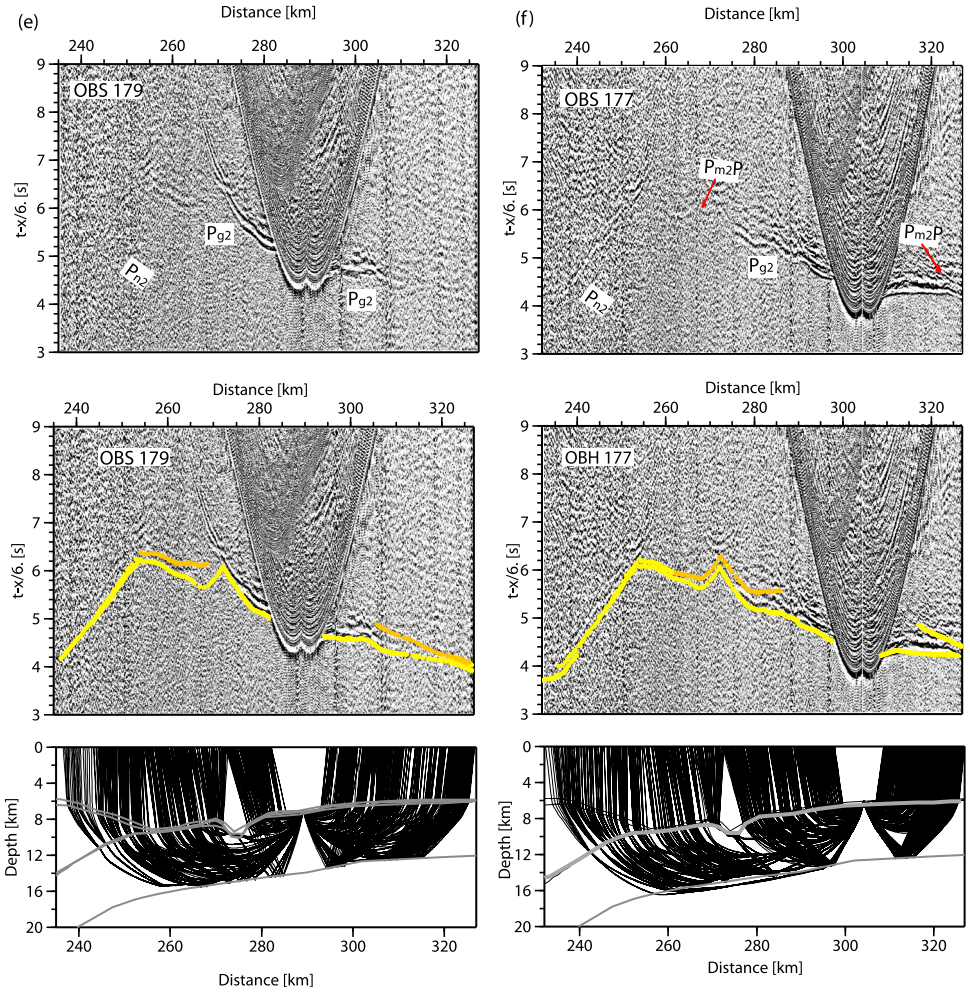

Figure 3. (continued)

10 so-called noisy arrival travel-time pick sets constructed by adding random phase errors (±50 ms) and common receiver errors (±50 ms) to the original data set [*Korenaga et al.*, 2000]. We then performed a tomographic inversion for each velocity model with one noisy data set, in order to estimate not only the dependence of the solution on the reference model, but also the effect of phase arrival time picking errors. The stopping criterion for each inversion was $\chi^2 \leq 1$, where χ^2 is the normalized sum of the RMS misfits divided by the corresponding picking uncertainties; a value of 1 means that the model error is equal to the data uncertainty.

[21] Figure 4b shows the Derivative Weight Sum (DWS), a proxy of the ray density of our velocity model [*Toomey and Foulger*, 1989]. Figure 4c shows the average velocity-depth model from the 100 final models, and detailed information regarding root-mean square travel-time misfits (T_{RMS}) and χ^2 parameters for the final average model is summarized in Table 1.

[22] Reflector and velocity uncertainties calculated from the 100 final velocity-depth models are shown in Figures 4d and 4e, respectively. The standard deviation (uncertainty) of the calculated velocities (ΔV_p) is generally well constrained for the overriding arc crust (Figure 4d). In the uppermost and lower part of the arc crust, ΔV_p values increase to greater than 0.1 km/s. In the uppermost mantle of the overriding plate and uppermost part of the Pacific oceanic crust, ΔV_p values increase up to 0.2 and 0.4 km/s, respectively. The average depth uncertainties of the Indo-Australian plate Moho is ±0.2 km, and reach maximum values larger than ±0.5 km at the westward edge of the velocity-depth model (Figure 4d), which is a zone characterized by the absence of $P_{m1}P$ reflections. Pacific plate Moho depth uncertainties were calculated at ±0.2 km east of the trench, while the top of the subducting Pacific crust is largely unconstrained below 10 km and where $P_{m2}P$ reflections are not clearly observed from 30–35 km depth (imaged zones in Figure 4c). We therefore interpolate both the top and bottom of the Pacific crust between the depths of <10 km and 30–35 km using the known geometry.

4.3. Description of Results

4.3.1. Subducting Pacific Plate

[23] The top of the oceanic basement is covered by a thin sedimentary cover of <200 m with velocities typical of pelagic sediments (1.6–1.9 km/s) [e.g., *Ito et al.*, 1995]. Reflections from the top and bottom of the subducting Pacific crust constrain the interplate boundary and oceanic Moho location, respectively. The average Pacific crustal

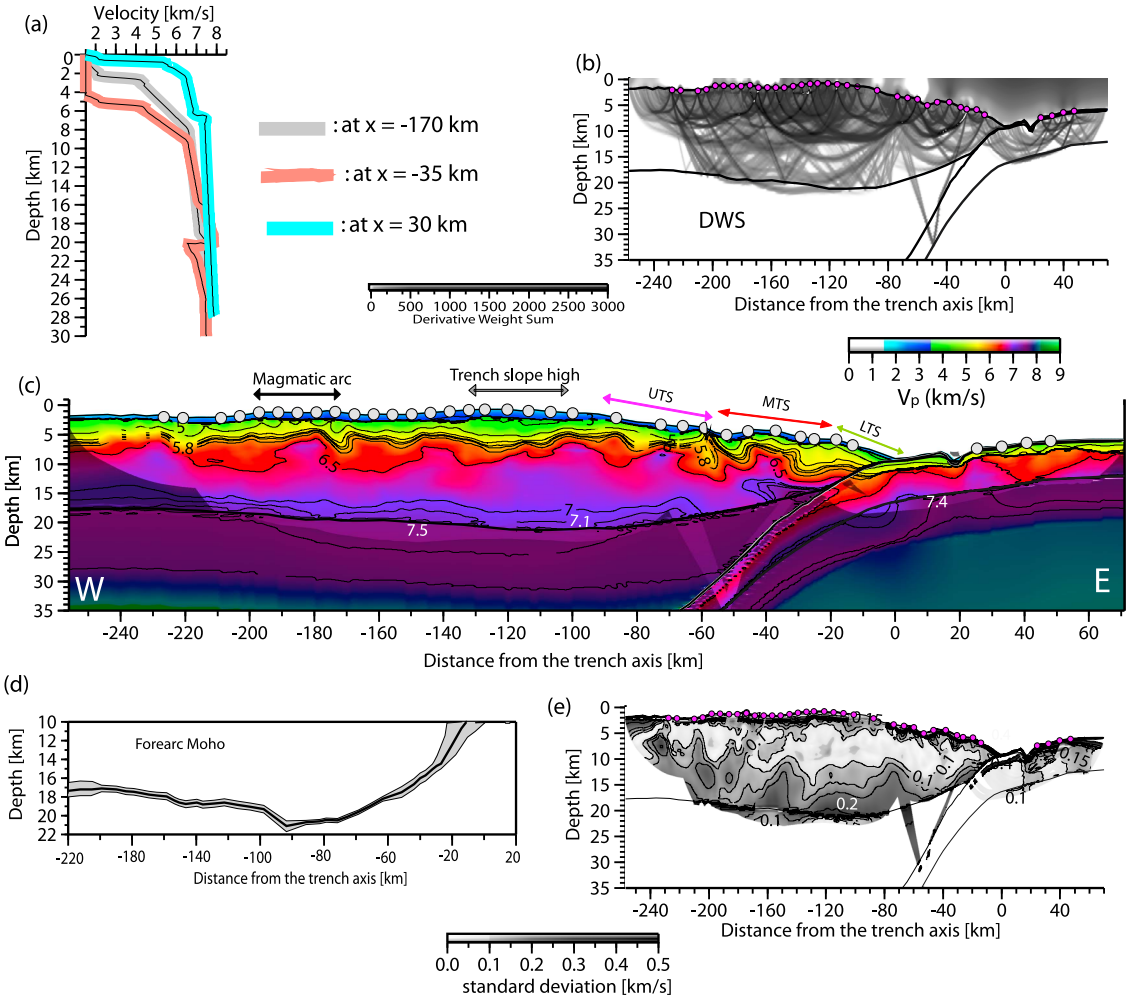

Figure 4. (a) Initial 1D velocity models constructed by forward modeling. (b) Derivative Weight Sum (DWS) for rays traveling throughout the model shown in Figure 4c. (c) Final velocity-depth model derived by averaging all Monte Carlo ensembles. UTS, MTS and LTS denote the upper, middle, and lower trench slopes, respectively. (d) Depth uncertainties for the fore-arc Moho. (e) Velocity uncertainty model based on Monte Carlo type realizations.

thickness is 6.0 ± 0.2 km (Figure 4). Similar thicknesses are found along the Tonga-Kermadec Trench at ~18.5°S [*Crawford et al.*, 2003] and at ~26°S [*Contreras-Reyes et al.*, 2010]. The average angle of subduction is ~30° which is similar to the shallow dip angle (depths <60 km) suggested by teleseismic hypocenter data [*Bonnardot et al.*, 2007].

[24] The oceanic crust consists of an upper layer ~1.5 km thick with velocities of 3.0–6.3 km/s, and a 3.0 to 3.5 km thick lower crust with velocities of 6.4–6.8 km/s. The oceanic mantle is characterized by extremely low velocities (~7.3 km/s), much lower than those typical of the uppermost mantle (≥8.0 km/s). A feature worth noting is located at 15–20 km east of the trench, where there is a graben in the downgoing plate which coincides with a region of extremely low crustal velocity and a thin upper crust (see Figure 5).

4.3.2. Overriding Australian Plate

[25] The Indo-Australian plate arc crust is covered by a sedimentary layer 1.0–1.5 km thick with seismic velocities ranging between 1.8 and 3.0 km/s, which is interpreted as a drape of pelagic and volcanoclastic sediments (Figure 4c). The volcanoclastic sediments are probably sourced from the arc volcanic front by debris flows and turbidity currents [*Clift et al.*, 1998]. Despite the steepness of the inner wall of the trench, the velocity model does not show a well-developed frontal prism of sediments at the trench. However, a fore-arc basin of up to 2 km thick appears to have formed 50–60 km arcward of the trench. The fore-arc basin is coincident with the onset of a ~2 km high scarp seen in the swath bathymetry data (Figure 6). This prominent feature is characterized by a sharp velocity contrast that propagates deep into the crust, and the outline of the discontinuity resembles a deep fault dipping toward the trench which is fairly coincident with the prominent scarp seen in the swath bathymetry data (Figure 5).

[26] A wedge-shaped body, with velocities ranging between 3.0 and <6.0 km/s, can be identified in the seismic velocity model, whose westward limit at 10–20 km from the

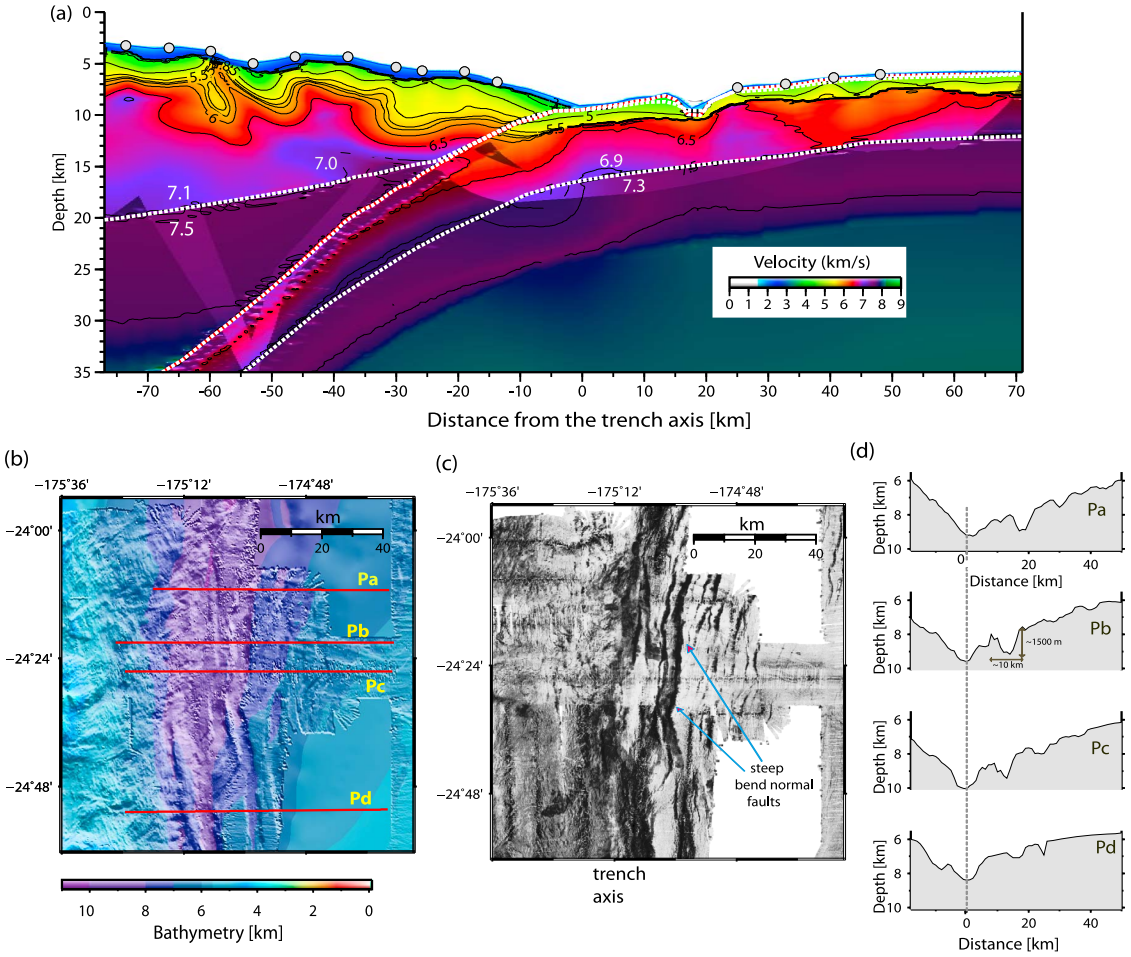

Figure 5. (a) Easternmost portion of the final velocity-depth model showing the trench-outer rise and trenchward-most part of the fore-arc regions. (b) High-resolution multibeam bathymetric mapping shows horst and graben structures caused by bending-related faulting aligned parallel to the trench axis. North of the collision zone between the Louisville Ridge and the trench, horst and graben fault systems are remarkably deep and wide. (c) Deep-towed side-scan sonar image showing large horst and graben structures in the outer rise region. (d) Depth profiles extracted from shipboard bathymetry along profiles shown in Figure 5b. Line Pb shows a graben 1.5 km deep and 10 km wide caused by tensional stresses due to strong bending of the old Pacific oceanic lithosphere.

trench axis coincides with a pronounced horizontal velocity gradient (Figure 6). Arcward of this strong velocity contrast, the velocity-depth model reveals an overriding arc crust with typical velocities of oceanic igneous rocks. That is, an upper crust with velocities of 3.8 to 6.5 km/s, and a lower crust with velocities of 6.5–7.1 km/s. In addition, one feature is notably absent: there is virtually no material within the arc with a velocity of 6.0 ± 0.4 km/s (Figure 7).

[27] The velocity-depth model reveals that the Indo-Australian plate crust thickens from trench to arc. The maximum crustal thickness is reached at the trench slope high which coincides with the shallowest seafloor along our profile. Here, the upper and lower crustal thickness are 5 and 15 km thick, respectively. In the vicinity of the magmatic arc, velocities in excess of 6.5 km/s are reached at the relatively shallow depth of 4 km below the seafloor. A similar feature is detected at the western end of the seismic profile. On the other hand, P_{n1} phases image the uppermost 2 km of the mantle wedge. Mantle velocities are clearly low (7.5 km/s) compared to average oceanic upper mantle velocities (≥8.0 km/s).

[28] We calculate travel times for some phases that are not clearly observed on the seismic record (Figures 3c–3f). For instance, the absence of $P_{m2}P$ reflections on the eastern side of OBS 191 (Figure 3c) and both sides of OBS 184 (Figure 3d) may be due to attenuated phase amplitudes as a consequence of the low mantle wedge velocities. The deep-seated reflector was forward modeled using a floating reflector as shown in Figure 3c, where the angle of incidence of ~60° is consistent with a velocity contrast of about 1 km/s. Similar features have been observed in the Izu-Bonin-Mariana arc [*Takahashi et al.*, 2008].

5. Gravity Modeling

[29] In order to better constrain the velocity structure along the seismic profile, we calculated the gravity effect of the seismic model and compared it to the observed free-air

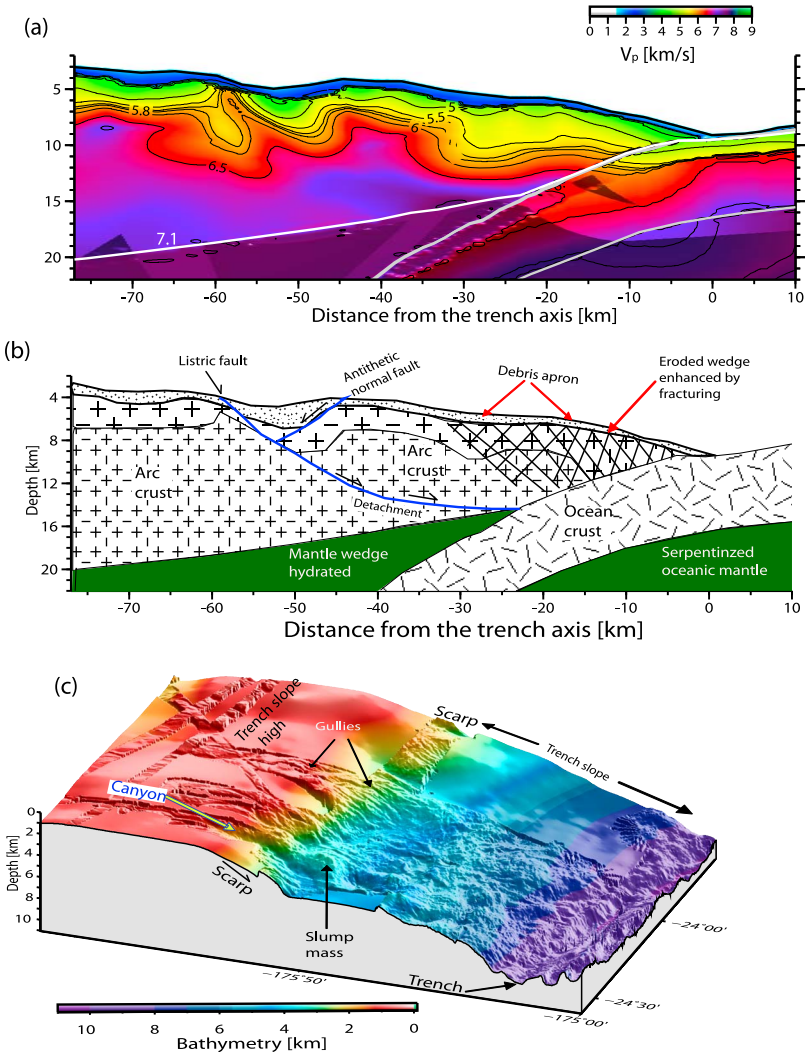

Figure 6. (a) Outer fore-arc region of the velocity-depth model. (b) The relatively low velocities (4.0–5.5 km/s) of the trenchward-most part of the fore-arc (the wedge) are interpreted as arc crust highly fractured by frontal and basal erosion, enhanced by subduction of large horst and graben and subduction of the Louisville Ridge over the last few million years. At ~55 km west of the trench axis, formation of a large scarp has enabled the development of a narrow fore-arc basin ~10 km wide and 2–3 km thick. Velocity discontinuities around the fore arc basin resemble deep crustal normal faults (blue curve). (c) Large scarp feature on the overriding Indo-Australian plate at 60 km offset from the trench axis, which spatially correlates with the velocity discontinuities shown in Figure 6a and is interpreted as a large-scale feature caused by extension (Figure 6b). The trench slope is highly eroded as evidenced by the presence of deep gullies. A flat, basinal area is fed by a canyon incising the trench slope.

gravity anomaly. Our 2D gravity calculation is based on *Parker*'s [1972] spectral method in which the seismic structure is approximated by a number of layers of uniform density contrast. We converted velocity (V_p) to density (ρ) using the following relationships:

Hamilton [1978] relationship for the sedimentary section

$$\rho = 1 + 1.18\left(V_p - 1.5\right)^{0.22}$$

Carlson and Herrick's [1990] relationship for igneous upper crust

$$\rho = 3.61 - \frac{6.0}{V_p}$$

Birch's [1961] law for plagioclase, and diabase-gabbro ecoglite (lower crust)

$$\rho = 0.375\left(1 + V_p\right)$$

[30] We derived a density model for transect P02 using the same layer boundary geometry as in our seismic velocity model. For the upper oceanic mantle densities we used the V_p versus ρ relationship of *Carlson and Miller* [2003], which accounts for the dependence of V_p with the degree of serpentinization, and we limited the density to a maximum of 3230 kg/m^3 for the deeper mantle region. First, we model the satellite-derived free-air gravity anomaly (FAA) [*Sandwell and Smith*, 1997] using only the seismically

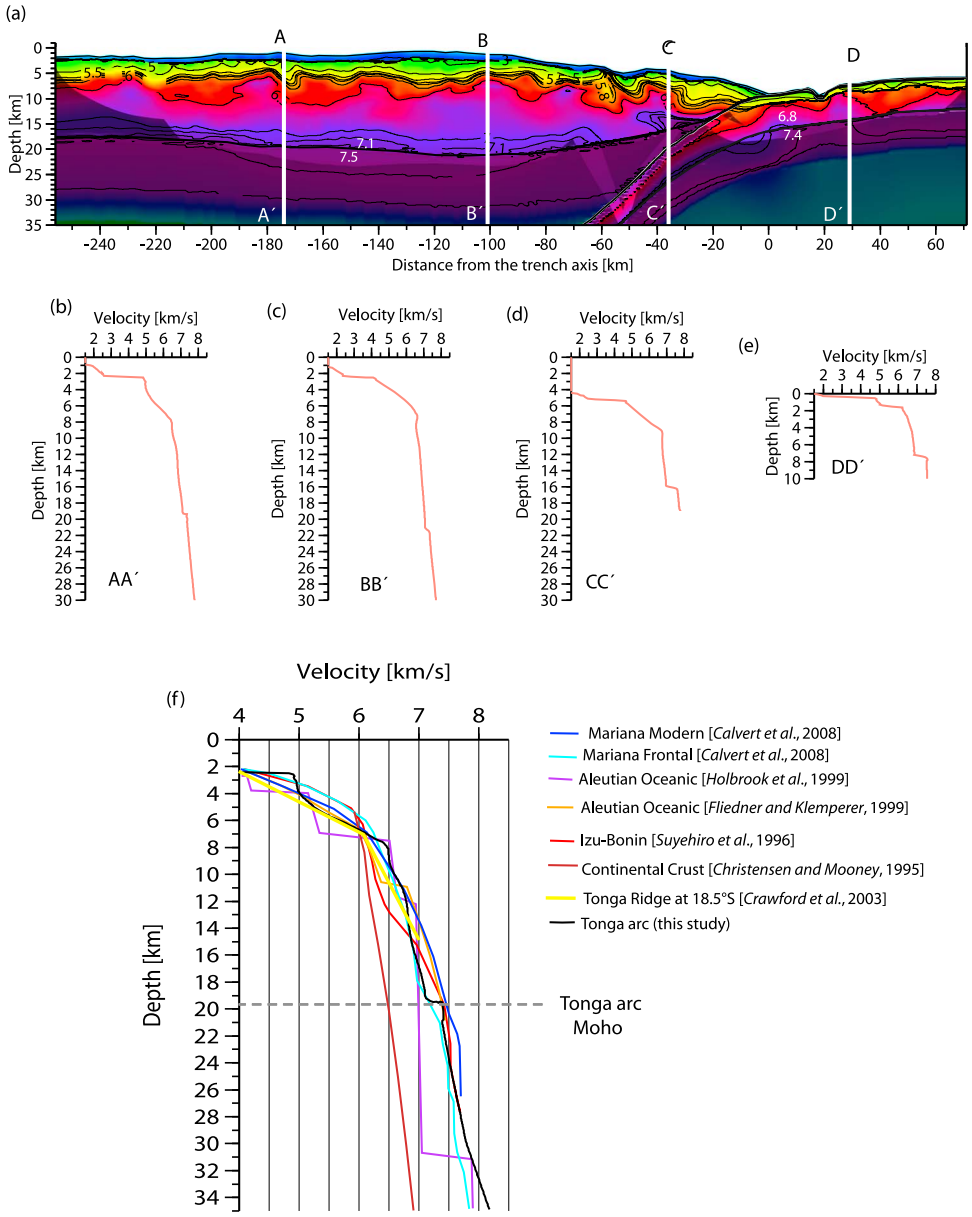

Figure 7. (a) Final velocity model showing locations of the velocity-depth profiles extracted and shown (b) at the magmatic front, (c) at the trench slope high, (d) at the trenchward part of the fore-arc and (e) at the outer rise (oceanic Pacific crust). (f) Comparison of average 1-D velocity functions from the Mariana, Izu-Bonin, Aleutian and Tonga oceanic island arcs and continental crust.

constrained parts of the model. That is, beyond the maximum depth of seismic penetration, we assumed a typical mantle density of 3300 kg/m^3 (Figure 8a). The results show a calculated anomaly that is 90 and 20 mGal higher, in the fore-arc and outer-rise respectively, than the observed anomaly (Figure 8). Secondly, we adopted an alternative model which is similar to the previous one except that we extended to larger depth at which typical mantle densities of 3300 kg/m^3 are restored and, thus, we allow a thicker section of low density serpentinized mantle (Figure 8b). The best fit is reached if the serpentinized mantle thicknesses for the Pacific and Indo-Australian lithospheres are ~25 km and ~40 km, respectively (Figure 8c). Our preferred density model has a RMS misfit of about 7 mGal and is consistent with mantle alteration and a deep hydrated mantle wedge.

6. Interpretation and Discussion

[31] We present an interpretive model of the Tonga subduction zone based on our high-resolution seismic tomographic velocity and gravity model (Figure 9). The principal features of this model are: (1) extremely low velocities both in the mantle wedge and uppermost oceanic Pacific mantle which are interpreted as reflecting mantle serpentinization, (2) existence of a prominent graben (1.5 km deep and 10 km wide) in the outer rise region, (3) a relative low velocity

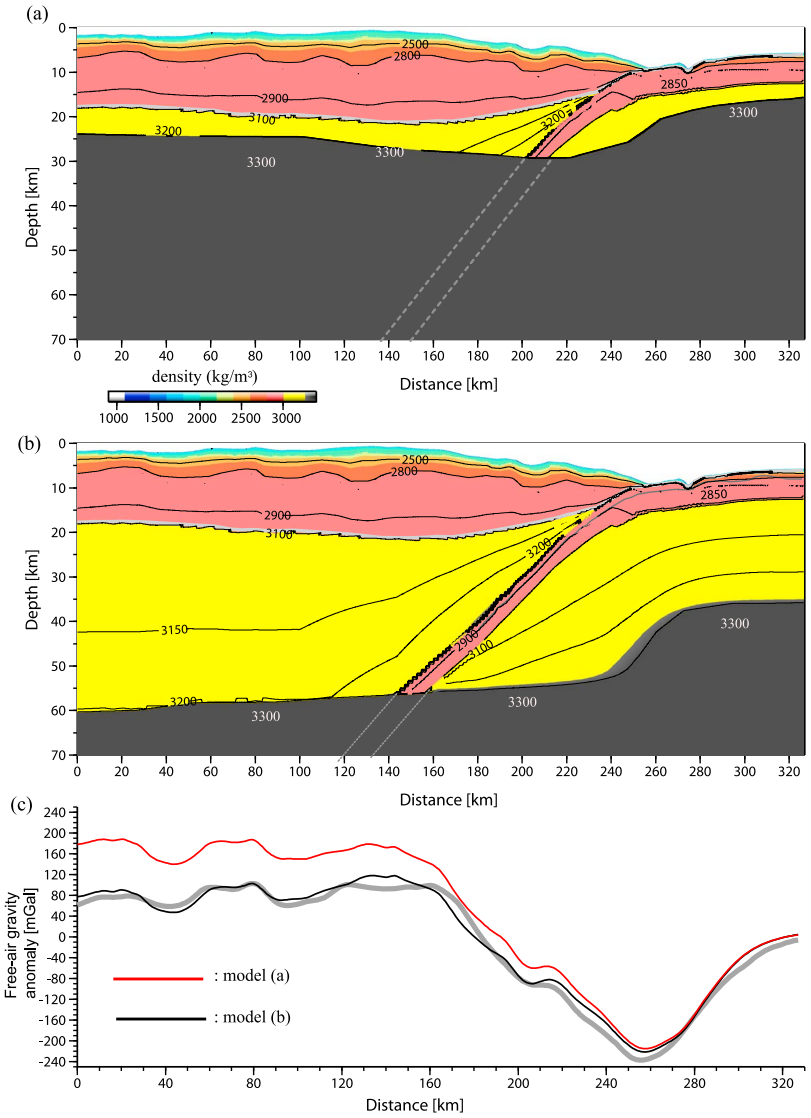

Figure 8. (a) Density model obtained by converting the velocities of the final best fit model to densities using only the seismically well-constrained parts of the model (illuminated regions in Figure 4c). In parts unconstrained by rays coverage, we assume a typical mantle density of 3300 kg/m^3. (b) Preferred density model obtained by converting velocities to densities, extending further into subsurface the depth of mantle having been serpentinized. (c) Grey thick curve is the observed free-air gravity anomaly (Δg), while red and black curves are the predicted free-air gravity anomaly using model and a and b, respectively. The average root mean square (RMS) residual anomaly for models a and b are ~52 and ~7 mGal, respectively.

region within the overriding plate located near the trench, (4) a prominent scarp located 60 km arcward of the trench, and (5) relative high velocities of 7.0–7.1 km/s for the Tonga lowermost arc crust. We will first discuss the underthrusting Pacific lithosphere and then the Indo-Australian overthrusting plate.

6.1. The Trench-Outer Rise Region

[32] In the trench-outer rise region, uppermost crustal velocities are lower than 3.5 km/s, and are atypical for the uppermost part of layer 2 of mature oceanic crust (>4.5 km/s) [e.g., *Grevemeyer and Weigel*, 1996]. Velocities lower than 7 km/s in the lower oceanic crust in the trench-outer rise area suggest a significant alteration of the porosity structure of the entire oceanic crust. The decrease in velocity is most likely accompanied by an increase in the degree of fracturing, coinciding with the prominent normal extensional faults caused by bending-related faulting (Figure 5). Mantle velocities are as low as 7.3 km/s (Figure 5a), which is significantly lower than the velocity of mantle peridotite (≥8.0 km/s). Low mantle velocities of 7.3 km/s indicate a high degree of serpentinization of about 30% [*Christensen*, 1996]. A possible mechanism responsible for percolation of seawater down to mantle depths is stress variation induced by the bending of the oceanic plate, producing sub-hydrostatic or even negative pressure gradients along normal faults, favoring downward pumping of fluids [*Faccenda et al.*, 2009].

[33] High-resolution swath bathymetric data image well-developed bend-faults which are oriented approximately

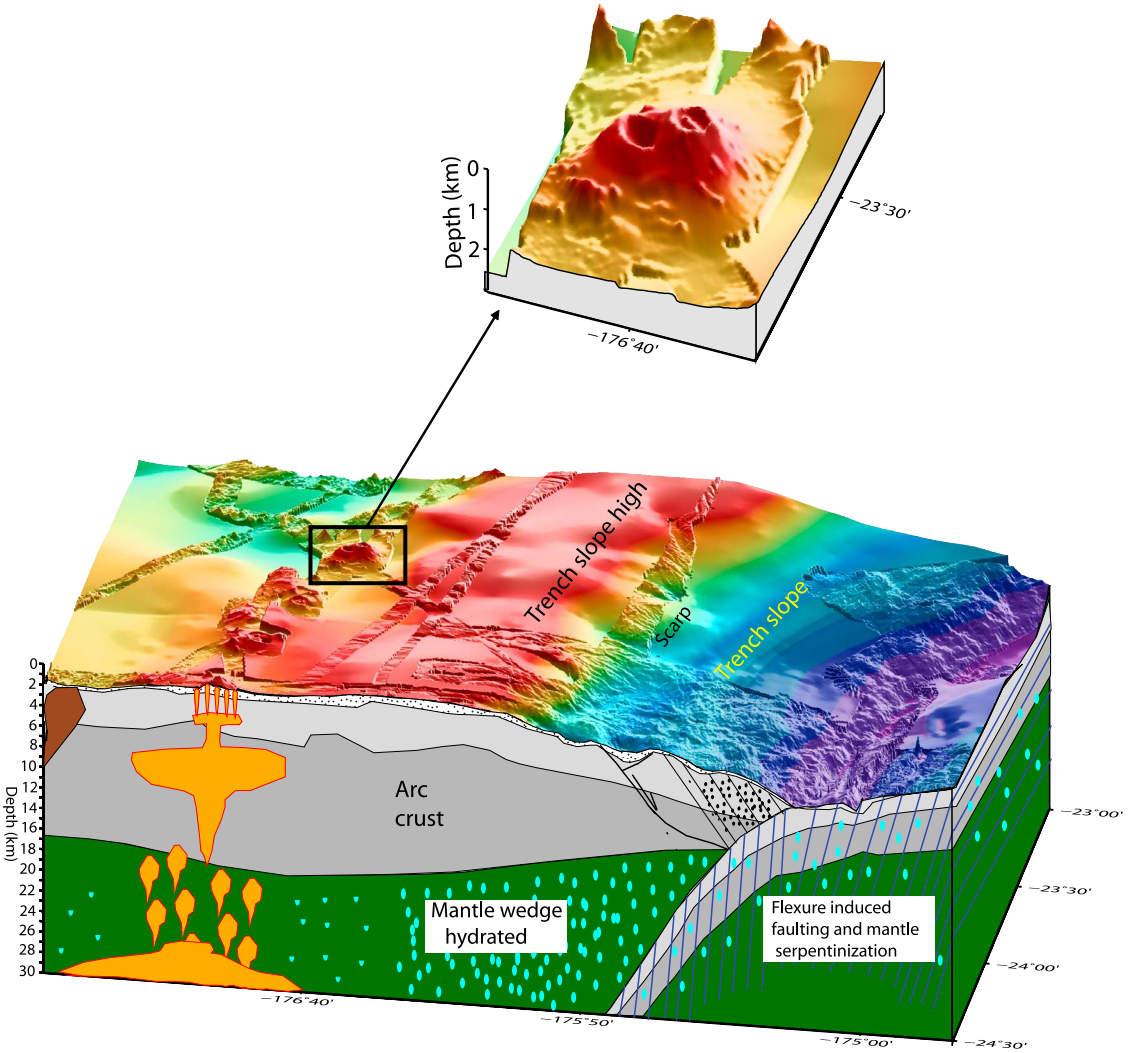

Figure 9. Summarized interpretation of the tomographic velocity model (Figure 4c). The highly hydrated Pacific plate subducts beneath the Indo-Australian plate at the Tonga Trench, with melt rising from the subducting slab to form the volcanic Tonga Ridge (the active Tonga arc). Dehydration reactions in the subducting crust promote mantle wedge hydration. The arc crust at the tip of the Indo-Australian plate is highly fractured by tectonic erosion. The outer fore-arc is affected by extension, where a huge scarp of 2 km offset has been formed trenchward of the trench slope high.

parallel to the trench axis (Figure 5). Similar features have been discussed off Chile [*Contreras-Reyes and Osses*, 2010], Central America [*Grevemeyer et al.*, 2007] and the Kuril Islands and Japan [*Kobayashi et al.*, 1998]. In particular, the remarkable graben in the Tonga trench-outer rise (~10 km wide and 1.5 km deep, Figure 5d) suggests that the uppermost layer of the oceanic lithosphere is pervasively fractured and likely hydrated, an inference supported by the extremely low crustal and mantle velocities. The modeled uppermost mantle velocities of 7.3 km/s are quite low, when compared with those observed in other outer rise settings such as Central America (7.3–7.6 km/s) [*Grevemeyer et al.*, 2007; *Ivandic et al.*, 2008, 2010], Sumatra (~7.6 km/s) [*Planert et al.*, 2010], and off Chile (~7.8 km/s) [*Contreras-Reyes et al.*, 2008].

[34] Old oceanic lithosphere is strong so it may bend into the trench over a wider distance across the plate boundary, possibly leading to a limited amount of brittle failure and hydration if bending stresses do not significantly exceed the yield strength of crustal rocks. Conversely, our geophysical data suggest deep faulting and hydration of the Pacific oceanic lithosphere. This apparent paradox can be explained by a potential deep location of the brittle-ductile transition for old oceanic lithosphere, which could lead to deeper hydration than in young subducting lithosphere. In fact, oceanic flexure studies and yield strength envelope considerations suggest that the effective elastic thickness of oceanic lithosphere and the depth to the brittle-ductile transition increases with the age [e.g., *Watts*, 2001]. According to these data [e.g., *Goetze and Evans*, 1979; *McNutt and Menard*, 1982] the transition is expected at ~40 km and ~25 km for oceanic lithosphere 80 Ma and 30 Ma, respectively. Thus, the increased depth to the brittle-ductile transition in older lithosphere might facilitate deeper hydration within the mantle if bending stresses exceed the yield strength of the lithosphere. This is reflected in the reduced

flexural rigidity in old oceanic plates off Kermadec [*Billen and Gurnis*, 2005] and off Chile [*Contreras-Reyes and Osses*, 2010], which have been interpreted as caused by intense fracturing and increase in fluid-pore pressure.

[35] On the other hand, the lower limit for mantle hydration may not necessarily be coincident with the lithospheric brittle-ductile transition. In fact, a tensional crack may promote migration of water into the mantle, while a compressional fault may not. *Contreras-Reyes et al.* [2008] used deep mantle refractions to image the upper mantle velocity structure of 30 Ma oceanic Nazca lithosphere, and obtained a maximum mantle serpentinization of 6–8 km within the upper mantle. These depths coincide with the isotherm of 300°–350°C according to the thermal model of *McKenzie et al.* [2005], which considers the effect of a variable thermal conductivity with age. The 300°–350°C isotherm is a good proxy for the neutral plane according the maximum depths of tensional events in the trench outer-rise region [*Seno and Yamanaka*, 1996]. Thus, the neutral plane appears to be the maximum depth at which mantle hydration occurs off Chile [*Contreras-Reyes and Osses*, 2010].

[36] Our gravity model (Figure 8) is consistent with a ~24 km thick upper mantle layer with low densities (3100–3220 kg/m^3) for the old Pacific lithosphere, suggesting deep-seated hydration. Moreover, the 300°–350°C isotherm depths are reached at ~30 km for 80 Ma old Pacific lithosphere according the thermal model of *McKenzie et al.* [2005], which is consistent with the maximum depth of reduced mantle densities. This result suggests that the neutral plane associated with an isotherm of 300°–350°C is a good approximation for the maximum depth limit of mantle serpentinization.

6.2. The Overriding Indo-Australian Plate

6.2.1. Tectonic Erosion Processes

[37] At erosive margins, trench fill is thinner than a few hundred meters and almost no sediment is frontally or basally accreted. Instead, upper plate material is removed, resulting in a high taper fore-arc and the continental or island arc basement positioned close to the trench. Basically, subduction erosion acts in two different ways: frontal erosion takes place at the tip of the fore-arc, and redistributes material that has been transported downslope by small- and large-scale debris flows. Basal tectonic erosion, in contrast is a process which scrapes off material from the base of the overriding fore-arc. Tectonic erosion is a common process in margins characterized by a fast subduction rate (>6.0 mm/a) and thin sedimentary trench fill (<1.0 km thick) [*Clift and Vannucchi*, 2004, and references therein]. Hence, the Tonga subduction zone provides favorable conditions for tectonic erosion. Indeed, data from Ocean Drilling Program Site 841 on the mid-trench slope of the Tonga fore-arc have shown a link between tectonic trenchward tilting and subsidence of the basement, which supports a model of basal erosion near the trench [*Clift and MacLeod*, 1999].

[38] *Ballance et al.* [1989] proposed a model of accelerated tectonic erosion caused by the subduction of the Louisville Ridge. They noted that the post-collision zone is remarkably deep (~10850 m) and the trench axis has migrated ~80 km arcward compared to the pre-collision zone (Figure 1). The collision zone is associated with a shallow trench (5–6 km depth) due to the Louisville Ridge (Figure 2). The Osbourn seamount, lies immediately east of the trench axis and will be the next edifice of the chain to collide with the fore-arc slope (Figure 2), as the collision zone moves rapidly southward at rates faster than 200 km/Ma [*Bevis et al.*, 1995]. *Ballance et al.* [1989] proposed that tectonic erosion has been accelerated in the post-collision zone of the Louisville Ridge with the Tonga Trench, where both frontal and basal erosion processes have caused subsidence of the trench slope due to oversteepening of the inner trench wall and crustal thinning, respectively.

[39] Our velocity-depth model shows a wedge-shaped body with relatively low velocities of 3.0–5.5 km/s compared to the 6.0–~7.1 km/s arc velocities imaged further westward (Figure 6a). This wedge-shaped body is coincident with the steep trench slope and is interpreted as highly fractured arc crust associated with tectonic erosion (Figure 6b), intensified by the subduction of the Louisville Ridge over the last few million years. The arcward limit of the wedge is marked by a pronounced horizontal velocity gradient as shown in Figure 6c. The pronounced but progressive decrease of seismic velocities trenchward suggests an increase in fracturing, metamorphism and degree of hydration. A similar feature has been observed in the northern erosional margin of Chile, where andesitic velocities decrease progressively toward the sediment-starved trench, from 5.5–6.0 to 4.0 km/s [*Sallares and Ranero*, 2005]. Contrastingly, in accretionary margins the margin wedge is characterized by abrupt seismic discontinuities interpreted as the contact between the frontal accretionary prism and the continental crust [*Contreras-Reyes et al.*, 2008]. The discontinuity of seismic velocities in accretionary margins rules out a progressive trenchward increase of fracturing intensity of the margin's inner basement as is usually seen in erosional margins. The arc wedge of Tonga is about 30 km wide and lacks the <3.5 km/s seismic velocities typical of frontal accretionary prisms [*Contreras-Reyes et al.*, 2008]. Sediment apron velocities lower than 3.0 km/s, however, are interpreted as reflecting mass-wasting products.

[40] A clear difference between the northern Chile and Tonga margins is the magnitude of the arc crust velocities. The Tonga arc has lowermost crustal velocities typical of a basaltic composition (~7.1 km/s), which are faster than typical lowermost continental crustal velocities of 6.0–6.2 km/s (Figure 7f). We summarize our interpretation in Figure 6b, which shows an igneous core not yet affected by vigorous erosion and displays typical velocities for oceanic crust with an extrusive and intrusive layer with velocities of 4.0–6.2 km/s and 6.3–7.1 km/s, respectively. Arc wedge velocities ranging from 4.0 and 5.5 km/s are interpreted as a highly eroded and fluid saturated arc crust. The eroded wedge was most likely followed by crustal thinning and steepening of the trench slope in the aftermath of Louisville Ridge seamount subduction.

6.2.2. The Tonga Forearc

[41] At approximately 60 km arcward of the trench, the velocity model shows a pronounced discontinuity where, just to the east, there is a 10 km wide fore-arc basin (Figure 6). We interpret this feature as a trenchward-dipping listric fault (Figure 6b). Extension can also be inferred from the bathymetric data where a major scarp with 2 km offset

might reflect the head scar of a landslide (Figure 6c). The scarp can be traced along the entire Tonga-Kermadec platform for more than 2000 km (Figure 1), though it is better developed north of the Louisville Ridge. The presence of such fault scarps has already been recognized in acoustic backscatter images [*Lonsdale*, 1986; *MacLeod and Lothian*, 1994; *Clift et al.*, 1998]. Active extension in the outer fore-arc and trench slope has also been inferred from the dominance of normal faults in cores recovered at ODP Site 841 [*MacLeod*, 1994]. Structural measurements show a progressive increase in dip with depth below seafloor and with age, which was interpreted in terms of basal erosion and progressive rotation of the fore-arc into the trench [*MacLeod*, 1994]. *MacLeod* [1994] noted that the overall increase in dip with age translates to a gradual rotation of the fore-arc trenchward, a feature attributed to collapse of the trench slope in the wake of the collision of the fore-arc with the Louisville Ridge.

[42] *MacLeod* [1994] showed that the initial effect of the Louisville Ridge collision with the trench was compression and uplift in the outer fore-arc, followed by gravitational collapse, extension and overstepping of the trench slope as a seamount is fully subducted. Alternatively, *Lallemand* [1998] has argued that strong coupling between the downgoing and overriding plates around the Pacific results in rapid tectonic erosion (4–10 km/m.y.) and hence extension and subsidence. However, the shallow and hydrated mantle wedge suggests that strong coupling is confined to the overriding subducting crust contact, which is the region more affected by erosion (Figure 6b). Here, erosion causes crustal thinning and hydro-fracturing of the fore-arc. Extension and gravitational collapse, however, span several ten of kilometers westward [e.g., *MacLeod and Lothian*, 1994], which may indicate that the erosive effect of the subducting Louisville Ridge, which extends several tens of kilometers arcward, also affects the fore-arc mantle of the Indo-Australian plate. Seismic data suggest that the internal structure of the Louisville Ridge comprises a dense, high velocity core [*Contreras-Reyes et al.*, 2010], which might vigorously erode the front and base of the upper plate.

[43] On the other hand, synchronous uplift of the outer arc high results in canyon development and down-cutting along the eastern edge of the Tonga platform [*Clift et al.*, 1998]. Coincidently, our seismic profile follows an incised canyon (Figure 6c).

6.2.3. The Arc Crust and Magmatic Arc

[44] The crustal thickness is highly variable along the Indo-Australian plate being maximum near the trench slope high where the total crustal thickness is about 20 km thick (Figure 4c). The region of maximum crustal thickness spatially correlates with the shallowest seafloor region indicating some degree of isostatic compensation. The thick crust in the trench slope high spatially correlates with the remnant arc and suggests that the locus of magmatism has migrated westward. Migration of the magmatic front is a typical feature observed in subduction zones affected by tectonic erosion [e.g., *Kukowski and Oncken*, 2006], which is the case in Tonga.

[45] Seismic velocities and the compositions of erupted lavas suggest that the Tonga arc crust has a mafic bulk composition, similar to accreted sections like Kohistan in Pakistan and Talkeetna in Alaska [e.g., *DeBari and Greene*, 2011], in contrast to the andesitic bulk composition of continents. The absence of material within the arc with velocities of 6.0 ± 0.4 km/s (typical velocities for upper continental crust) suggests that the Tonga arc has a predominantly basaltic composition. Figure 7 shows the comparison of velocities in the Tonga arc to those of (1) average continental crust [*Christensen and Mooney*, 1995], (2) the Mariana arc [*Calvert et al.*, 2008], (3) Aleutian arc [*Holbrook et al.*, 1999; *Fliedner and Klemperer*, 1999], (4) Izu-Bonin arc [*Suyehiro et al.*, 1996], and (5) Tonga Ridge at ~18.5°S [*Crawford et al.*, 2003]. The average continental crust has a substantially lower proportion of mafic material in the lower crust than the Tonga arc crust has, and the continental crust has a distinct mid-crustal layer with velocities of 6.1–6.4 km/s (granite), which is lacking in the Tonga crust. However, the arc crust for Aleutian, and Marianas has a MORB-type relative composition like Tonga (Figure 7). Therefore, if island arcs form a significant source of continental crust, the bulk properties of arc crust must be substantially modified during or after accretion to a continental margin [*Holbrook et al.*, 1999]. The pervasive deformation, plutonic processes and delamination of a mafic-to-ultramafic residuum necessary to transform arc crust into mature continental crust probably occurs during arc-continent collision or through subsequent establishment of a continental arc [*Holbrook et al.*, 1999].

[46] The nature of the Tonga fore-arc might also be important to test models of subduction initiation. *Stern and Bloomer* [1992] and *Bloomer et al.* [1994] have suggested that incipient (Eocene) arc crust, which presently seems to be exposed in the Tonga fore-arc, formed by foundering of the Pacific plate, causing extension and intense melting in the overriding plate. Our velocity model shows that the thickest arc crust is located 200–250 km trenchward from the Lau spreading center, suggesting that initial arc magmatism activity occupied a much broader zone and crustal production was more intense. Thus, it appears that arc crust produced by extensive decompression melting associated with subduction initiation, as suggested by the conceptual model of *Stern and Bloomer* [1992], is found along the Tonga fore-arc.

[47] A remarkable feature of the Tonga arc imaged by our seismic velocity model is the relative high velocity zone under the active volcanic front, where high lower crustal velocities of ~7.1 km/s are observed at shallow depths (Figure 4c). This high velocity zone may represent arc-related intrusions, perhaps at a level from which mid-crustal magma chambers feed surface eruptions. In the back-arc, a similar feature is observed and may be sourced from the Lau basin spreading center further west or by the abundance of plutons.

6.2.4. Mantle Wedge Hydration

[48] Low fore-arc mantle velocities (~7.5 km/s) and densities (3150–3230 kg/m^3) suggests hydration of the fore-arc mantle wedge (Figures 4c and 8). Large volumes of aqueous fluids must be released upwards by dehydration reactions in the wet subducting oceanic Pacific lithosphere. As discussed in section 6.1, the altered Pacific oceanic crust might contain a large volume of free water in pore spaces and bound water in hydrous minerals promoting mantle wedge hydration.

Geophysical evidence for serpentinized fore-arc mantle has been reported from a number of subduction zones including Alaska, Aleutians, central Andes, Cascadia, Izu-Bonin-Mariana, and central Japan [see *Hyndman and Peacock*, 2003].

[49] The main factors controlling fluid production beneath the fore-arc mantle are the convergence rate, the thickness of the fore-arc crust (i.e., fore-arc Moho depth), and the amount of water in the incoming crust and sediments [*Hyndman and Peacock*, 2003]. The rate at which free and bound water enters a subduction zone is approximately proportional to the convergence rate and inversely proportional to the overriding crustal thickness. For thick upper plate crust, more of the water goes into the fore-arc crust, rather than the fore-arc mantle. Thus, more fluid may be available for hydration of the mantle wedge in island arc settings than in continental subduction zones. Naturally, the degree of serpentinization will also be controlled by the amount of water stored within the subducting lithosphere. Thus, taking into account these three factors for the Tonga subduction zone, we can conclude that this region has the optimal conditions for vigorous mantle wedge hydration. These conditions are: (1) fast convergence rate (~200 mm/a), (2) a relative thin arc crust 15–20 km thick, and (3) a highly hydrated subducting Pacific oceanic lithosphere.

[50] Alternatively, the low fore-arc mantle velocities may be due to melts frozen in the mantle (magmatic underplating). In fact, seismological and petrological studies indicate the presence of cumulates and restites, produced during crustal growth, below the Moho [*Takahashi et al.*, 2008]. Also low fore-arc mantle velocities can be caused by melt inclusions in the mantle [*Lizarralde et al.*, 2004]. In addition, the presence of a deep-seated reflector within the fore-arc mantle may indicate the transfer of the lower crustal residues to the upper mantle across the Moho or lower velocity materials, as has been interpreted for the Izu-Bonin-Mariana arc [*Takahashi et al.*, 2008].

7. Conclusions

[51] The combined analysis of seismic wide-angle seismic data, shipboard bathymetry and gravity data, reveals the velocity and density structure of the incoming-subducting Pacific and overriding Indo-Australian plates north of the modern collision zone of the Louisville Ridge and Tonga Trench.

[52] 1. Crustal and mantle velocities are extremely low, indicating a highly fractured and hydrated oceanic Pacific lithosphere. In addition, extensional outer rise and fault-bounded half-graben faults have been mapped in the igneous basement, defining the onset of bending-related faulting. Some graben are as wide as 10 km and up to 1.5 km deep. It is possible that tensional faulting, and hence hydration, reaches depths of up to 30 km in the upper mantle as evidenced by low mantle densities (~3200 kg/m^3).

[53] 2. At the trenchward edge of the Indo-Australian plate, velocities in the range of 4.0–5.5 km/s suggest a highly hydro-fractured arc crust due to tectonic erosion. Erosion was accelerated after the subduction of the Louisville Ridge causing crustal thinning, overstepping of the inner trench slope and subsidence of the outermost fore-arc. Further arcward, arc crustal velocities are representative of basaltic composition suggesting an absence of erosion.

[54] 3. A large scarp (2 km offset) is coincident with velocity discontinuities resembling extensional faults. The scarp is associated with large-scale slope failure of the fore-arc.

[55] 4. The Tonga arc crust ranges in thickness between 7 and 20 km. The maximum crustal thickness is reached at the trench slope high suggesting isostatic compensation. Typical continental crust velocities of 6.0 ± 0.4 km/s are notably absent. Instead, crustal velocities suggest a basaltic composition. Crustal intrusion, and perhaps the presence of a magmatic chamber beneath the volcanic front, is inferred from shallow lower crustal velocities of ~7.1 km/s at a depth of ~4 km.

[56] 5. Fore-arc mantle velocities are as low as 7.5 km/s suggesting hydration of the mantle wedge or presence of melts frozen in the mantle. Gravity anomaly data are consistent with a low mantle density layer of ~40 km thick.

[57] **Acknowledgments.** We thank the captain, crew, and technical staff of MV *SONNE* cruise SO195 for their help at sea. This work was supported by the German Ministry of Education and Research (BMBF), grant 03G0195A and UK Natural Environmental Research Council (NERC) grant NE/F005318/1. We wish to acknowledge the useful comments and suggestions from Harm Van Avendonk, an anonymous reviewer, Marcelo Farías, Daniel Carrizo, and the Editor André Revil.

References

ANCORP Working Group (1999), Seismic reflection image revealing offset of Andean subduction-zone earthquake locations into oceanic mantle, *Nature*, *397*, 341–344.

Ballance, P. F., D. W. Scholl, T. L. Vallier, and R. H. Herzer (1989), Subduction of a Late Cretaceous seamount of the Louisville Ridge at the Tonga Trench: A model of normal and accelerated tectonic erosion, *Tectonics*, *8*, 953–962.

Bevis, M., et al. (1995), Geodetic observations of very rapid convergence and back-arc extension at the Tonga arc, *Nature*, *374*, 249–251.

Billen, M. I., and M. Gurnis (2005), Constraints on subducting plate strength within the Kermadec trench, *J. Geophys. Res.*, *110*, B05407, doi:10.1029/2004JB003308.

Birch, F. (1961), The velocity compressional waves in rocks to 10 kilobars, part 2, *J. Geophys. Res.*, *66*, 2199–2224.

Bloomer, S. H., A. Ewart, J. M. Hergt, and W. B. Bryan (1994), Geochemistry and origin of the igneous rocks from the outer Tonga forearc (site 841), *Proc. Ocean Drill. Program Sci. Results*, *135*, 625–646.

Bonnardot, M.-A., M. Regnier, E. Ruellan, C. Christova, and E. Tric (2007), Seismicity and state of stress within the overriding plate of the Tonga-Kermadec subduction zone, *Tectonics*, *26*, TC5017, doi:10.1029/2006TC002044.

Calvert, A. J., S. L. Klemperer, N. Takahashi, and B. C. Kerr (2008), Three-dimensional crustal structure of the Mariana island arc from seismic tomography, *J. Geophys. Res.*, *113*, B01406, doi:10.1029/2007JB004939.

Carbotte, S. M., and D. S. Scheirer (2004), Variability of ocean crustal structure created along the global mid-ocean ridge, in *Hydrogeology of Oceanic Lithosphere*, edited by E. E. Davis and H. Elderfield, pp. 128–150, Cambridge Univ. Press, New York.

Carlson, R. L. (2003), Bound water content of the lower oceanic crust estimated from modal analyses and seismic velocities of oceanic diabase and gabbro, *Geophys. Res. Lett.*, *30*(22), 2142, doi:10.1029/2003GL018213.

Carlson, R. L., and C. N. Herrick (1990), Densities and porosities in the oceanic crust and their variations with depth and age, *J. Geophys. Res.*, *95*, 9153–9170.

Carlson, R. L., and D. J. Miller (2003), Mantle wedge water contents estimated from seismic velocities in partially serpentinized peridotites, *Geophys. Res. Lett.*, *30*(5), 1250, doi:10.1029/2002GL016600.

Christensen, N. I. (1996), Poisson's ratio and crustal seismology, *J. Geophys. Res.*, *101*, 3139–3156, doi:10.1029/95JB03446.

Christensen, N. I., and W. D. Mooney (1995), Seismic velocity structure and composition of the continental crust: A global view, *J. Geophys. Res.*, *100*, 9761–9788.

Clift, P. D., and C. J. MacLeod (1999), Slow rates of subduction erosion estimated from subsidence and tilting of the Tonga forearc, *Geology*, *27*, 411–414.

Clift, P., and P. Vannucchi (2004), Controls on tectonic accretion versus erosion in subduction zones: Implications for the origin and recycling of the continental crust, *Rev. Geophys.*, *42*, RG2001, doi:10.1029/2003RG000127.

Clift, P. D., C. J. MacLeod, D. R. Tappin, D. J. Wright, and S. H. Bloomer (1998), Tectonic controls on sedimentation and diagenesis in the Tonga Trenchand forearc, southwest Pacific, *Geol. Soc. Am. Bull.*, *110*, 483–496.

Collot, J. Y., and B. Davy (1998), Forearc structures and tectonic regimes at the oblique subduction zone between the Hikurangi Plateau and the southern Kermadec margin, *J. Geophys. Res.*, *103*, 623–650.

Contreras-Reyes, E., and A. Osses (2010), Lithospheric flexure modeling seaward of the Chile trench: Implications for oceanic plate weakening in the Trench Outer Rise region, *Geophys. J. Int.*, *182*, 97–112, doi:10.1111/j.1365-246X.2010.04629.x.

Contreras-Reyes, E., I. Grevemeyer, E. R. Flueh, and C. Reichert (2008), Upper lithospheric structure of the subduction zone offshore of southern Arauco peninsula, Chile, at 38°S, *J. Geophys. Res.*, *113*, B07303, doi:10.1029/2007JB005569.

Contreras-Reyes, E., I. Grevemeyer, A. B. Watts, L. Planert, E. R. Flueh, and C. Pierce (2010), Crustal intrusion beneath the Louisville hotspot track, *Earth Planet. Sci. Lett.*, *289*, 323–333, doi:10.1016/j.epsl.2009.11.020.

Crawford, W. C., J. A. Hildebrand, L. M. Dorman, S. C. Webb, and D. A. Wiens (2003), Tonga Ridge and Lau Basin crustal structure from seismic refraction data, *J. Geophys. Res.*, *108*(B4), 2195, doi:10.1029/2001JB001435.

DeBari, S. B., and A. Greene (2011), Vertical stratification of composition, density, and inferred magmatic processes in exposed arc crustal sections, in *Arc-Continent Collision*, edited by D. Brown and P. Ryan, pp. 121–144, Springer, Berlin.

Faccenda, M., T. V. Taras, and L. Burlini (2009), Deep slab hydration induced by bending-related variations in tectonic pressure, *Nat. Geosci.*, *2*, 790–793, doi:10.1038/ngeo656.

Fliedner, M., and S. L. Klemperer (1999), Structure of an island arc: Wide-angle seismic studies in the eastern Aleutian Islands, Alaska, *J. Geophys. Res.*, *104*, 10,667–10,694.

Goetze, C., and B. Evans (1979), Stress and temperature in the bending lithosphere as constrained by experimental rock mechanics, *Geophys. J. R. Astron. Soc.*, *59*, 463–478.

Grevemeyer, I., and W. Weigel (1996), Seismic velocities of the uppermost igneous crust versus age, *Geophys. J. Int.*, *124*, 631–635, doi:10.1111/j.1365-246X.1996.tb07041.x.

Grevemeyer, I., C. R. Ranero, E. R. Flueh, D. Klaeschen, and J. Bialas (2007), Passive and active seismological study of bending-related faulting and mantle serpentinization at the Middle America trench, *Earth Planet. Sci. Lett.*, *258*, 528–542, doi:10.1016/j.epsl.2007.04.013.

Hacker, B. R. (2008), H2O subduction beyond arcs, *Geochem. Geophys. Geosyst.*, *9*, Q03001, doi:10.1029/2007GC001707.

Hacker, B. R., S. M. Peacock, G. A. Abers, and S. D. Holloway (2003), Subduction factory: 2. Are intermediate-depth earthquakes in subducting slabs linked to metamorphic dehydration reactions?, *J. Geophys. Res.*, *108*(B1), 2030, doi:10.1029/2001JB001129.

Hamilton, E. L. (1978), Sound velocity-density relations in the sea-floor sediments and rocks, *J. Acoust. Soc. Am.*, *63*, 366–377.

Hawkins, J. W. (1995), Evolution of the Lau Basin: Insights from ODP 135, in *Active Margins and Marginal Basins of the Western Pacific*, *Geophys. Monogr. Ser.*, vol. 88, edited by B. Taylor and J. Natland, pp. 125–173, AGU, Washington, D. C.

Holbrook, W. S., D. Lizarralde, S. McGeary, N. Bangs, and J. Diebold (1999), Structure and composition of the Aleutian island arc and implication for continental crustal growth, *Geology*, *27*, 31–34.

Hyndman, R. D., and S. M. Peacock (2003), Serpentinization of the forearc mantle, *Earth Planet. Sci. Lett.*, *212*, 417–432, doi:10.1016/S0012-821X(03)00263-2.

Ito, G., M. McNutt, and R. Gibson (1995), Crustal structure of the Tuamotu Plateau, 15°S, and implications for its origin, *J. Geophys. Res.*, *100*, 8097–8114.

Ivandic, M., I. Grevemeyer, A. Berhorst, E. R. Flueh, and K. McIntosh (2008), Impact of bending related faulting on the seismic properties of the incoming oceanic plate offshore of Nicaragua, *J. Geophys. Res.*, *113*, B05410, doi:10.1029/2007JB005291.

Ivandic, M., I. Grevemeyer, J. Bialas, and C. J. Petersen (2010), Serpentinization in the trench-outer rise region offshore of Nicaragua: Constraints from seismic refraction and wide-angle data, *Geophys. J. Int.*, *180*, 1253–1264, doi:10.1111/j.1365-246X.2009.04474.x.

Karig, D. E. (1970), Ridges and basins of the Tonga-Kermadec island arc system, *J. Geophys. Res.*, *75*, 1443–1470.

Kobayashi, K., M. Nakanishi, K. Tamaki, and Y. Ogawa (1998), Outer slope faulting associated with the western Kuril and Japan trenches, *Geophys. J. Int.*, *134*, 356–372.

Korenaga, J., W. S. Holbrook, G. M. Kent, P. B. Kelemen, R. S. Detrick, H. C. Larsen, J. R. Hopper, and T. Dahl-Jensen (2000), Crustal structure of the southeast Greenland margin from joint refraction and reflection seismic tomography, *J. Geophys. Res.*, *105*, 21,591–21,614.

Kukowski, N., and O. Oncken (2006), Subduction erosion: The "normal" mode of forearc material transfer along the Chilean margin?, in *Frontiers in Earth Sciences*, vol. 3, *The Andes: Active Subduction Orogeny*, edited by O. Oncken et al., pp. 217–236, Springer, Berlin.

Lallemand, S. E. (1998), Possible interaction between mantle dynamics and high rates of arc consumption by subduction processes in Circum-Pacific area, in *Mantle Dynamics and Plate Interactions in East Asia*, *Geodyn. Ser.*, vol. 27, edited by M. F. J. Flower et al., pp. 1–9, AGU, Washington, D. C.

Lizarralde, D., J. B. Gaherty, J. A. Collins, G. Hirth, and S. D. Kim (2004), Spreading-rate dependence of melt extraction at mid-ocean ridges from mantle seismic refraction data, *Nature*, *432*, 744–747, doi:10.1038/nature03140.

Lonsdale, P. (1986), A multibeam reconnaissance of the Tonga trench axis and its intersection with the Louisville chain, *Mar. Geophys. Res.*, *8*, 295–327.

MacLeod, C. J. (1994), Structure of the outer Tonga forearc at Site 841, *Proc. Ocean Drill. Program Sci. Results*, *135*, 313–329.

MacLeod, C. J., and A. Lothian (1994), Comparison of GLORIA sidescan sonar and core-derived structural data from Site 841, Tonga Trench, *Proc. Ocean Drill. Program Sci. Results*, *135*, 373–382.

McKenzie, D., J. Jackson, and K. Priestley (2005), Thermal structure of oceanic and continental lithosphere, *Earth. Planet. Sci. Lett.*, *233*, 337–349.

McLennan, S. M., and S. R. Taylor (1982), Geochemical constraints on the growth of the continental crust, *J. Geol.*, *90*, 347–361.

McNutt, M. K., and H. W. Menard (1982), Constraints on yield strength in the oceanic lithosphere derived from observations of flexure, *Geophys. J. R. Astron. Soc.*, *71*, 363–394.

Parker, R. L. (1972), The rapid calculation of potential anomalies, *Geophys. J. R. Astron. Soc.*, *31*, 447–455.

Parsons, B., and J. Sclater (1977), An analysis of the variation of ocean floor bathymetry and heat flow with age, *J. Geophys. Res.*, *82*, 803–827.

Planert, L., H. Kopp, E. Lueschen, C. Mueller, E. R. Flueh, A. Shulgin, Y. Djajadihardja, and A. Krabbenhoeft (2010), Lower plate structure and upper plate deformational segmentation at the Sunda-Banda arc transition, Indonesia, *J. Geophys. Res.*, *115*, B08107, doi:10.1029/2009JB006713.

Ruellan, E., J. Delteil, I. Wright, and T. Matsumoto (2003), From rifting to active spreading in the Lau Basin-Havre Trough backarc system (SW Pacific): Locking/unlocking induced by seamount chain subduction, *Geochem. Geophys. Geosyst.*, *4*(5), 8909, doi:10.1029/2001GC000261.

Ruepke, L. R., J. P. Morgan, M. Hort, and J. A. D. Connolly (2004), Serpentine and the subduction zone water cycle, *Earth Planet. Sci. Lett.*, *223*, 17–34.

Sallares, V., and C. R. Ranero (2005), Structure and tectonics of the erosional convergent margin off Antofagasta, north Chile (23 300S), *J. Geophys. Res.*, *110*, B06101, doi:10.1029/2004JB003418.

Sandwell, D. T., and W. H. F. Smith (1997), Marine gravity anomaly from Geosat and ERS-1 satellite altimetry, *J. Geophys. Res.*, *102*, 10,039–10,054.

Seno, T., and Y. Yamanaka (1996), Double seismic zones, compressional deep trench-outer rise events and superplumes, in *Subduction: Top to Bottom*, *Geophys. Monogr. Ser.*, vol. 96, edited by G. Bebout et al., pp. 347–355, AGU, Washington, D. C.

Shipboard Scientific Party (1992), Site 841, *Proc. Ocean Drill. Program, Initial Rep.*, *135*, 571–660.

Stern, R. J., and S. H. Bloomer (1992), Subduction zone infancy: Examples from the Eocene Izu-Bonin-Mariana and Jurassic California arcs, *Geol. Soc. Am. Bull.*, *104*, 1621–1636.

Suyehiro, K., N. Takahashi, Y. Ariie, Y. Yokie, R. Hino, M. Shinohara, T. Kanazawa, N. Hirata, H. Tokuyama, and A. Taira (1996), Continental crust, crustal underplating, and low-Q upper mantle beneath an oceanic island arc, *Science*, *272*, 390–392.

Takahashi, N., S. Kodaira, Y. Tatsumi, Y. Kaneda, and K. Suyehiro (2008), Structure and growth of the Izu-Bonin-Mariana arc crust: 1. Seismic constraint on crust and mantle structure of the Mariana arc-back-arc system, *J. Geophys. Res.*, *113*, B01104, doi:10.1029/2007JB005120.

Toomey, D., and G. Foulger (1989), Tomographic inversion of local earthquake data from the Hengill-Grensdalur central volcano complex, Iceland, *J. Geophys. Res.*, *94*, 17,497–17,510.

Ulmer, P., and V. Trommsdorff (1995), Serpentine stability to mantle depths and subduction-related magmatism, *Science*, *268*, 858–861.

Van Avendonk, H., A. Harding, J. Orcutt, and J. McClain (1998), A two-dimensional tomographic study of the Clipperton transform fault, *J. Geophys. Res.*, *103*, 17,885–17,899.

Watts, A. B. (2001), *Isostasy and Flexure of the Lithosphere*, 458 pp., Cambridge Univ. Press, New York.

Watts, A. B., J. K. Weissel, R. A. Duncan, R. L. Larson (1988), Origin of the Louisville Ridge and its relationship to the Eltanian fracture zone system, *J. Geophys. Res.*, *93*, 3051–3077.

Zelt, C. A. (1999), Modelling strategies and model assessment for wide-angle seismic traveltime data, *Geophys. J. Int.*, *139*, 183–204.

E. Contreras-Reyes, Departamento de Geofísica, Facultad de Ciencias Físicas y Matemáticas, Universidad de Chile, Blanco Encalada 2002, Santiago, Chile. (econtreras@dgf.uchile.cl)

E. R. Flueh, I. Grevemeyer, S. Moeller, and C. Papenberg, IFM-GEOMAR, Leibniz-Institut für Meereswissenchaften an der Universität Kiel, Wischhofstr. 1-3, D-24148 Kiel, Germany.

C. Peirce, Department of Earth Sciences, Durham University, South Road, Durham DH1 3LE, UK.

A. B. Watts, Department of Earth Sciences, University of Oxford, Parks Road, Oxford OX1 3PR, UK.